# NOTES AND CORRESPONDENCE

## Coupled Kelvin-Wave and Mirage-Wave Instabilities in Semigeostrophic Dynamics

PAUL J. KUSHNER

*Program in Atmospheric and Oceanic Sciences, Princeton University, Princeton, New Jersey*

MICHAEL E. MCINTYRE

*Centre for Atmospheric Science* at the Department of Applied Mathematics and Theoretical Physics, University of Cambridge, Cambridge, United Kingdom*

THEODORE G. SHEPHERD

*Department of Physics, University of Toronto, Toronto, Ontario, Canada*

19 August 1996 and 10 March 1997

ABSTRACT

A weak instability mode, associated with phase-locked counterpropagating coastal Kelvin waves in horizontal anticyclonic shear, is found in the semigeostrophic (SG) equations for stratified flow in a channel. This SG instability mode approximates a similar mode found in the Euler equations in the limit in which particle-trajectory slopes are much smaller than $f/N$, where $f$ is the Coriolis frequency and $N > f$ the buoyancy frequency. Though weak under normal parameter conditions, this instability mode is of theoretical interest because its existence accounts for the failure of an Arnol'd-type stability theorem for the SG equations. In the opposite limit, in which the particle motion is purely vertical, the Euler equations allow only buoyancy oscillations with no horizontal coupling. The SG equations, on the other hand, allow a physically spurious coastal ''mirage wave,'' so called because its velocity field vanishes despite a nonvanishing disturbance pressure field. Counterpropagating pairs of these waves can phase-lock to form a spurious ''mirage-wave instability.'' Closer examination shows that the mirage wave arises from failure of the SG approximations to be self-consistent for trajectory slopes $\gtrsim f/N$.

### 1. Introduction

Kushner and Shepherd (1995a,b) and Kushner (1995) have derived Arnol'd-type linear and nonlinear stability theorems for shear flows obeying the semigeostrophic (SG) equations (Hoskins 1975), using SG wave-activity conservation laws. These theorems fail to apply when the shear is horizontal and anticyclonic and when lateral boundaries are present, implying one of two possibilities. The first is that the flow is stable, but not provably stable by Arnol'd's method; the second is that the flow is unstable. In section 2 of this note we show, at least for constant shear, that the second alternative holds. The flow is unstable via a normal-mode instability that, under conditions commonly of interest, is exceedingly weak and spectrally confined. This SG instability is physically realistic in the sense that it closely resembles a similar instability mode of the Euler equations, for appropriate parameter values. It represents a destabilization of an otherwise stable anticyclonic shear flow by the presence of lateral boundaries. Mathematically, the theory is like the Eady theory of baroclinic instability, in which a vertical shear flow is destabilized by the presence of lower and upper boundaries. Physically, the instability can be interpreted in terms of phase-locked, counterpropagating coastal Kelvin waves (section 4).

The SG instability is physically realistic when the particle-trajectory slopes are sufficiently shallow. When the trajectory slopes are steepened by increasing $|k/m|$, where $k$ is the horizontal wavenumber and $m$ is the vertical wavenumber, the SG instability ceases to be physically realistic. In the limit $|k/m| \to \infty$, the SG instability becomes a wholly spurious instability, an artifact of the approximations in the SG equations (though still part of what is relevant to the question of SG Arnol'd stability). This finding prompts a more general

* The Centre for Atmospheric Science is a joint initiative of the Department of Chemistry and the Department of Applied Mathematics and Theoretical Physics.

*Corresponding author address:* Dr. Paul J. Kushner, Program in Atmospheric and Oceanic Sciences, Forrestal Campus, Princeton University, Princeton NJ 08544.
E-mail: pjk@gfdl.gov

analysis of the SG equations' accuracy in representing neutral boundary-trapped waves over possibly steep topography (section 3). That analysis shows, in particular, that the spurious instability solution for $|k/m| \to \infty$ can be attributed to the phase locking of counterpropagating pairs of neutral waves that are likewise artifacts of approximations in the SG equations. In the case of a vertical wall, these neutral waves have zero particle motion though nonzero disturbance pressure, an interestingly bizarre consequence of the inconsistency of the SG approximations in the regime considered. For this reason we call these waves ''mirage waves,'' and the associated instability a ''mirage-wave instability.''

## 2. Horizontal-shear instability in the presence of lateral boundaries

Consider the shear flow $\tilde{u} = \tilde{u}_y y$ with constant horizontal shear $\tilde{u}_y$, between two walls at $y = \pm L/2$ in a Boussinesq, stratified fluid with constant buoyancy frequency $N$ on an $f$ plane, with $|\tilde{u}_y| < f < N$. This flow has constant potential vorticity. We focus on barotropic effects and so take the fluid to be unbounded vertically as well as in the alongstream direction. The flow is provably stable for cyclonic but not for anticyclonic shear, according to the SG stability theorems mentioned in the introduction. We assume anticyclonic shear, $\tilde{u}_y > 0$, and look for normal-mode instabilities. Note that this flow would be provably stable under the SG equations if one or both of the bounding walls were absent.

The linearized SG equations are given in the appendix. From (A.1)–(A.5) it may be shown that the disturbance satisfies

$$p'_{xx} + \frac{p'_{yy}}{1 - \tilde{u}_y/f} + \frac{f^2 p'_{zz}}{N^2} = 0, \tag{2.1}$$

where $p'$ is the disturbance pressure and suffixes denote derivatives. This corresponds to the vanishing of the disturbance potential vorticity, as can be shown from the equations in Hoskins (1975). From (A.1), the boundary condition of no normal flow at each wall implies

$$\tilde{D}p'_y = fp'_x \quad \text{at} \quad y = \pm L/2, \tag{2.2}$$

where $\tilde{D} = \partial_t + \tilde{u}\partial_x$.

Solutions of the form

$$p' = \hat{p}(y) \exp\{i(kx + mz - \omega t)\}, \tag{2.3}$$

with $0 < k < \infty$, are substituted into (2.1)–(2.2). The resulting equations are nondimensionalized by scaling lengths $y$ and $1/k$ by the cross-channel width $L$, height $1/m$ by $fL/N$, velocity $\tilde{u}$ by the cross-channel velocity difference $U = \tilde{u}_y L$, and time $t$ by $L/U$. Nondimensionalized quantities will be denoted by subscript ''$*$.'' With the Rossby number defined as

$$\epsilon = U/(fL) = \tilde{u}_y/f, \tag{2.4}$$

the nondimensional equation for $\hat{p}(y)$ is

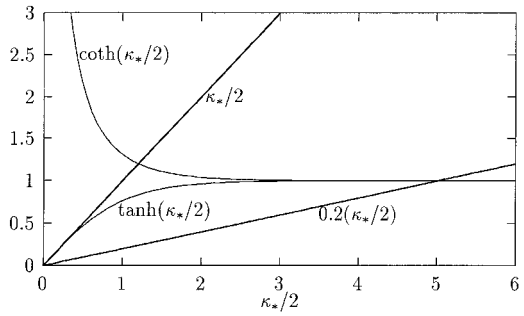


FIG. 1. Graphs of coth($\kappa_*/2$), tanh($\kappa_*/2$), and $\epsilon\kappa_*/2$ for $\epsilon = 1$ and $\epsilon = 0.2$, showing in particular the exponential smallness of the instability window as $\epsilon \to 0$ (sloping line rotating clockwise).

$$\hat{p}_{*_{y_*y_*}} - \kappa_*^2 \hat{p}_* = 0, \tag{2.5}$$

where

$$\kappa_*^2 = (1 - \epsilon)k_*^2 + (1 - \epsilon)m_*^2. \tag{2.6}$$

The boundary conditions are

$$\epsilon\hat{\omega}_* \hat{p}_{*_{y_*}} + k_* \hat{p}_* = 0 \quad \text{at } y_* = \pm 1/2, \tag{2.7}$$

with the nondimensional intrinsic frequency defined by

$$\hat{\omega}_* = \omega_* - k_* y_*. \tag{2.8}$$

The SG eigenvalue problem (2.5) with (2.6), (2.7) is mathematically analogous to the classic Eady (1949) problem of baroclinic instability, generalized to sloping boundaries. The eigenvalues of (2.5) with (2.6), (2.7) are given by

$$\frac{\omega_*}{k_*} = \pm\frac{1}{\epsilon\kappa_*}\sqrt{\left(\frac{\epsilon\kappa_*}{2} - \coth[\kappa_*/2]\right)\left(\frac{\epsilon\kappa_*}{2} - \tanh[\kappa_*/2]\right)}, \tag{2.9}$$

which are either pure real or pure imaginary. Graphical solution (Fig. 1) shows (a) that, for all $\epsilon$ with $0 < \epsilon < 1$, (2.9) predicts instability for some window of $\kappa_*$ values and hence for all values of the ratio $k_*/m_*$, and (b) that when $\epsilon$ is fixed (with $0 < \epsilon < 1$) and $k_*$, $m_*$ varied, growth rates maximize for $|k_*/m_*| \to \infty$.

Figure 1 also shows that for small $\epsilon$ the unstable window is narrow and weak, in fact, exponentially narrow and weak, in the limit $\epsilon \to 0$. Figure 2a shows a numerical example, for $\epsilon = 0.2$ (see caption for details). The instability window has width $\Delta\kappa = 0.0002L^{-1}$ and maximum nondimensional growth rate $\sim 5 \times 10^{-5}$. When $f = 10^{-4}$ s$^{-1}$ so that $L/U = (\epsilon f)^{-1} = 5 \times 10^4$ s, the dimensional $e$-folding time associated with this growth rate $\sim 10^9$ s $\sim$ 30 years.

A corresponding instability can be found in the Boussinesq Euler (nonhydrostatic) equations. As outlined in the appendix, the eigenvalue problem for the same basic flow can be shown to be

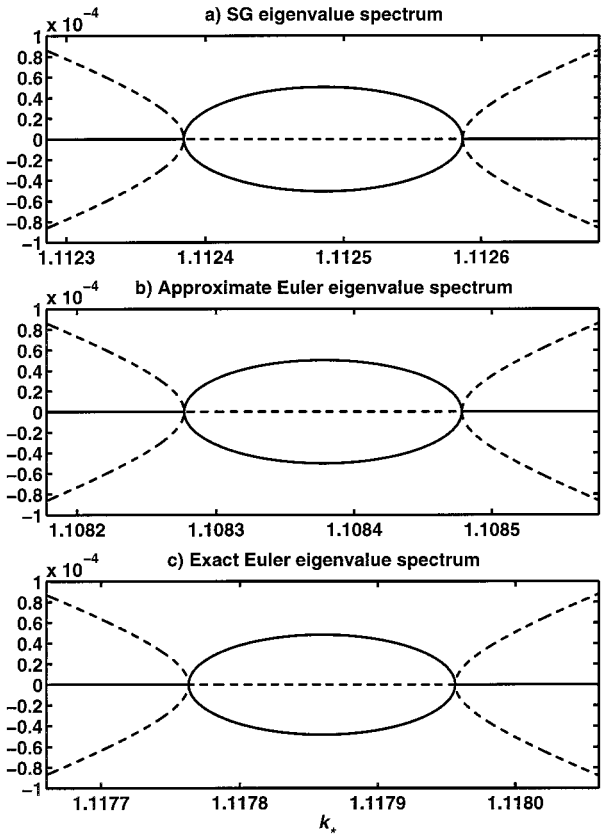


FIG. 2. Complex eigenvalue spectrum $\omega_*$ against $k_*$ for (a) SG eigenvalue problem (2.5) with (2.6), (2.7), solved analytically; (b) approximate Euler eigenvalue problem (2.5) with (2.12), (2.7), also solved analytically; (c) exact Euler eigenvalue problem (2.10) with (2.11), (2.7), solved numerically for 1000 values of $k_*$. Solid lines: $\omega_{*i}$. Dashed lines: $\omega_{*r}$. The positive branch of values of $\omega_{*i}$ and $\omega_{*r}$ was obtained by initializing the shooting code with positive values of $\omega_{*i}$ and $\omega_{*r}$, and the negative branch obtained by initializing with negative values. In the figure, the ratio $k_*/m_* = 0.1$ and $\epsilon = 0.2$. Note that $\kappa_* \cong 10$, and $\exp\{-\kappa_*\} \sim 10^{-4}$.

$$\hat{p}_{*y_*y_*} + A\hat{p}_{*y_*} + B\hat{p}_* = 0, \tag{2.10}$$

where

$$A = -\frac{2\epsilon^2 k_* \hat{\omega}_*}{1 - \epsilon - \epsilon^2\hat{\omega}_*^2},$$

$$B = -\frac{1 + \epsilon - \epsilon^2\hat{\omega}_*^2}{1 - \epsilon - \epsilon^2\hat{\omega}_*^2}k_*^2 - \frac{1 - \epsilon - \epsilon^2\hat{\omega}_*^2}{1 - \epsilon^2(f/N)^2\hat{\omega}_*^2}m_*^2. \tag{2.11}$$

From (A.9)–(A.10), it can be seen that the boundary condition (2.7) remains unchanged. This eigenvalue problem is close to the SG eigenvalue problem when $O(\epsilon^2|\hat{\omega}_*|)$ and $O(\epsilon^2|\hat{\omega}_*|^2)$ terms can be neglected. Then (2.10) reduces to the form (2.5) with (2.6) replaced by

$$\kappa_*^2 = (1 + 2\epsilon)k_*^2 + (1 - \epsilon)m_*^2 \tag{2.12}$$

and with the same boundary condition (2.7). The eigenvalue expression (2.9) now holds with $\kappa_*$ defined by (2.12) instead of (2.6). The only difference between (2.6) and (2.12) lies in the factor multiplying $k_*^2$. For $|k_*/m_*| \ll 1$ (that is, $|k/m| \ll f/N$) this represents only an $O[\epsilon(k_*/m_*)^2]$ discrepancy between the two eigenvalue problems.

Figure 2b shows the complex eigenvalue spectrum for the approximate Euler problem, (2.5) with (2.12), (2.7), and the same parameter values as before. Figure 2c shows the spectrum for the exact Euler problem, (2.10) with (2.11), (2.7). The exact Euler problem was solved numerically using the shooting algorithm of Press et al. (1992). The results illustrate that the SG and the approximate and exact Euler solutions all agree closely when $\epsilon$ is small and $|k_*/m_*| \ll 1$.

On the other hand, in the limit in which $|k_*/m_*| \to \infty$ for fixed $\epsilon$, in which limit the SG solution's growth rate is maximized, the Euler and the SG solutions disagree qualitatively. For both the Euler and the SG solutions in this limit, the disturbance quantities become independent of $z$, and the horizontal disturbance velocity $(u', v')$ becomes nondivergent. For the Euler solution, the horizontal disturbance velocity also becomes irrotational, implying that a disturbance streamfunction $\psi'$ may be defined with $(u', v') = (-\psi'_y, \psi'_x)$ and $\psi'_{xx} + \psi'_{yy} = 0$. This may be checked by substitution into $\partial_x$(A.10)–$\partial_y$(A.9) and use of $\tilde{D} = -i\omega + ik\tilde{u} \neq 0$. By the no-normal-flow boundary condition, $\psi'$ is constant on each boundary for every $z$. Since $\psi'$ is harmonic and proportional to $\exp(ik_*x_*)$ with $k_*$ nonzero, it follows that the horizontal disturbance velocity vanishes. Therefore, for the Euler solution, the disturbance pressure vanishes [by (A.9) since, again, $k_* \neq 0$ and hence $\partial_x \neq 0$]. Equations (A.11) and (A.5) still permit nonhydrostatic, purely vertical buoyancy oscillations with frequency $N$ in this limit, but because the disturbance pressure is zero the oscillations are uncoupled horizontally. By contrast, for the SG solution in this same limit $|k_*/m_*| \to \infty$, the disturbance pressure does not vanish. The reasons for this contrast are examined in the next section.

## 3. Mirage and other boundary-trapped waves

Consider a stratified resting fluid bounded to one side by a flat wall tilted into the $yz$ plane. Rhines (1970) has discussed the topographic neutral-wave solutions of the Euler equations in this geometry. We here compare Rhines' Euler solutions with the corresponding SG solutions, in the spirit of Allen et al.'s (1990) comparison of coastal Kelvin waves in the shallow-water equations with and without the SG approximations. We also, for completeness, consider the corresponding solutions of the Euler equations with the hydrostatic approximation.

We follow the conventions of Rhines (1970), who uses tilted coordinates $(x_1, x_2, x_3)$ and corresponding velocities $(u_1, u_2, u_3)$ such that the bounding wall is at

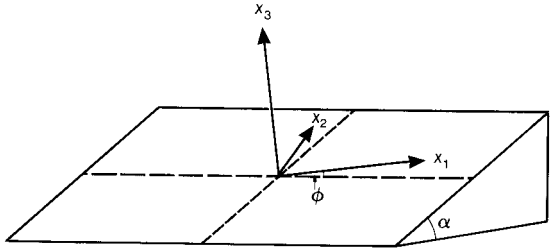


FIG. 3. Definition of titled coordinates, after Rhines (1970). The fluid occupies $x_3 > 0$.

$x_3 = 0$, and the $x_1$ and $x_2$ axes are rotated through an angle $\phi$ from the alongslope and upslope directions (see Fig. 3). All quantities are here understood to be dimensional. The corresponding linearized equations are given in the appendix.

We seek solutions of the form

$$\exp\{-\kappa x_3\}\ \exp\{(ik_3x_3 + ik_2x_2 - i\omega t)\}, \tag{3.1}$$

which, when $\kappa > 0$, represent boundary-trapped waves propagating in the $\pm x_2$ direction on the slope, and where it is now convenient to keep $\omega > 0$ and to allow $k_2$, assumed nonzero, to have either sign. This leads to

$$\frac{\omega}{f} = S|\sin\alpha\ \sin\phi| \tag{3.2}$$

$$\frac{\kappa}{k_2} = \frac{S(1 - \sin^2\alpha\ \sin^2\phi)\ \mathrm{sgn}(\sin\alpha\ \sin\phi)}{\cos^2\alpha + S^2\ \sin^2\alpha\ \cos^2\phi} \tag{3.3}$$

$$\frac{k_3}{k_2} = \frac{(S^2 - 1)\ \sin\alpha\ \cos\alpha\ \cos\phi}{\cos^2\alpha + S^2\ \sin^2\alpha\ \cos^2\phi}, \tag{3.4}$$

where for the Euler equations[1]

$$S = N/f, \tag{3.5}$$

for the hydrostatic Euler equations (HE)

$$S = \frac{N/f}{\sqrt{1 - \sin^2\alpha\ \sin^2\phi}}, \tag{3.6}$$

and for the SG equations

$$S = \frac{N/f}{\sqrt{1 + [(N/f)^2 - 1]\sin^2\alpha\ \sin^2\phi}}. \tag{3.7}$$

The waves always propagate in one direction only: toward the left as one looks up the slope (Rhines 1970).

We wish to determine the accuracy of the HE and SG solutions relative to the Euler solution. Inspection of (3.6) and (3.7) suggests that natural small parameters upon which to base series expansions are $\sin^2\alpha\ \sin^2\phi$ for the HE solution and $(N/f)^2\ \sin^2\alpha\ \sin^2\phi$ for the SG solution. Assuming $N/f \gg 1$, we find that

$$\frac{\omega_{\mathrm{HE}}}{\omega_{\mathrm{Euler}}} = 1 + O(\sin^2\alpha\ \sin^2\phi),$$

$$\frac{\omega_{\mathrm{SG}}}{\omega_{\mathrm{Euler}}} = 1 + O((N/f)^2\ \sin^2\alpha\ \sin^2\phi), \tag{3.8}$$

$$\frac{\kappa_{\mathrm{HE}}}{\kappa_{\mathrm{Euler}}} = 1 + O(\sin^2\alpha\ \sin^2\phi),$$

$$\frac{\kappa_{\mathrm{SG}}}{\kappa_{\mathrm{Euler}}} = 1 + O((N/f)^2\ \sin^2\alpha\ \sin^2\phi), \tag{3.9}$$

$$\frac{k_{3\mathrm{HE}}}{\kappa_{3\mathrm{Euler}}} = 1 + O(\sin^2\alpha\ \sin^2\phi),$$

$$\frac{k_{3\mathrm{SG}}}{k_{3\mathrm{Euler}}} = 1 + O((N/f)^2\ \sin^2\alpha\ \sin^2\phi). \tag{3.10}$$

The SG and the HE solutions break down as the slope of the particle trajectories, given approximately by $\sin\alpha\ \sin\phi$ [and exactly by $\sin\alpha\ \sin\phi(1 - \sin^2\alpha\ \sin^2\phi)^{-1/2}$], becomes too large. In order for the solutions to be accurate, the trajectory slope has to be much smaller than unity for the HE equations and much smaller than $f/N$ for the SG equations.

Returning to the geometry and dimensional notation of section 2, consider the limiting case of a vertical wall with $\alpha = +\pi/2$ and therefore, from (A.12), $(x_1, x_2, x_3) = (x\ \cos\phi + z\ \sin\phi, -x\ \sin\phi + z\ \cos\phi, -y)$. This corresponds to a version of Fig. 3 in which the wall is raised to the vertical, $y$ now points into the wall and out of the fluid (as with the channel wall at $y = L/2$ in section 2), and $x$ points horizontally to the right and $z$ vertically up the wall. Thus, (3.1) becomes

$$\exp\{\kappa y\}\ \exp\{-ik_3y + ik_2(-x\ \sin\phi + z\ \cos\phi) - i\omega t\}. \tag{3.11}$$

We see that the $x$-wavenumber $k = -k_2\ \sin\phi$, the $z$-wavenumber $m = k_2\ \cos\phi$, and $k_2^2 = k^2 + m^2$. Equations (3.2)–(3.4) with (3.5) reduce to

$$\omega_{\mathrm{Euler}} = \frac{N|k|}{\sqrt{k^2 + m^2}}, \qquad \kappa_{\mathrm{Euler}} = -\frac{f\sqrt{k^2 + m^2}\ \mathrm{sgn}(k)}{N},$$

$$k_{3\mathrm{Euler}} = 0. \tag{3.12}$$

We require $\kappa > 0$, and hence $k < 0$, for the disturbance to vanish in the limit $y \to -\infty$, that is, far from the wall. With $k < 0$, the expressions in (3.12) correspond to coastal Kelvin waves propagating in the $-x$ direction, which for $|k/m| \ll 1$ become nondispersive, with trapping scale normal to the wall $N/(f|m|)$, and well approximated by HE. The same waves are well approximated by SG only when $|k/m| \ll f/N$. The waves are then ''semigeostrophic'' in the literal sense of being geostrophically balanced in the direction away from the wall while maintaining unbalanced (gravity wave) motion along the wall. For $|k/m| \ll f/N$, the trapping scale normal to the wall is much smaller than the wavelength

[1] Note the sign error in Eq. (1.8) of Rhines (1970), as compared with (3.4) with (3.5) here.

along the wall. These are the same anisotropic conditions that make the SG equations appropriate for the analysis of frontal dynamics (Hoskins and Bretherton 1972; Hoskins 1975).

With $\alpha$ still $\pi/2$ so that the wall is still vertical, consider now the case $\phi \to \pi/2$, implying $k \to -k_2$ and $m \to 0$. This corresponds to the limit in which $|k_*/m_*| \to \infty$ (that is, $|k/m| \to \infty$), discussed at the end of section 2, in which the Euler and the SG solutions disagreed qualitatively. All disturbance quantities again become independent of $z$, and for the Euler equations the argument showing the vanishing of the horizontal ($xy$) disturbance velocity field ($u'$, $v'$) and the disturbance pressure field $p'$ still applies. [Alternatively, any solution of the form (3.11) and with $v' = 0$ at the wall must have $v' = 0$ everywhere; then $\partial_x u' = iku' = 0$, by (A.14) with $\partial_z = 0$, implying that $u' = 0$, because $k \neq 0$, and thence, through (A.13), that $p' = 0$.] So all the disturbance fields except $w'$ and $\rho'$ vanish, and as in section 2 we again have nonhydrostatic, purely vertical buoyancy oscillations with frequency $\omega = N$, uncoupled horizontally.

The corresponding SG solution, in this limiting case, is again qualitatively different from the Euler solution, and more evidently unphysical than the SG solution discussed at the end of section 2. Like the Euler solution, the SG solution has vanishing horizontal velocity ($u'$, $v'$). But in contrast with the Euler solution, the SG solution has a nonzero disturbance pressure $p' \propto \exp\{\kappa y\} \exp\{ikx - i\omega t\}$, with $\kappa = -k > 0$. The SG solution is therefore still a boundary-trapped wave in this limit, with decay scale $|k|^{-1}$. This boundary-trapped wave is the ''mirage wave.''

The vanishing of the ($u'$, $v'$) field, despite the nonvanishing of the $p'$ field, can be regarded as the result of an exact cancellation between the geostrophic and ageostrophic velocities. It is easy to check that these fields do indeed satisfy the SG equations (A.1)–(A.6). The frequency of the mirage wave is $\omega = f$, as can be seen at once from (3.2) with the limiting form of (3.7), $S = 1$. Therefore, in (A.1)–(A.2), $\tilde{D} = \partial_t = -if$, and from the form of $p'$ we have also $p'_x = -ip'_y$ so that recalling also the definitions of $u'_g$ and $v'_g$, and that ($u'$, $v'$) = (0, 0), we see that the equations are indeed satisfied. Another point of contrast with the Euler solution is that, for the SG solution, $\rho' = 0$, by (A.3) with $\partial_z = im = 0$, and hence $w' = 0$, by (A.5). Therefore, the mirage wave has motionless particles in the presence of a nonvanishing disturbance pressure.

For the HE, but not the SG equations, (A.14)–(A.16) may be used to show that the same limit $|k/m| \to \infty$ yields only the trivial solution with all disturbance fields vanishing. This is quite unlike the mirage wave with its vanishing disturbance velocity and nonvanishing disturbance pressure.

## 4. Interpretation

The instabilities described in section 2 may be interpreted in terms of the coupling and phase locking of counterpropagating pairs of boundary-trapped waves of the kind discussed in section 3 (e.g., Lighthill 1963, pp. 92–93; Cairns 1979; Hoskins et al. 1985; Sakai 1989). For $\epsilon \ll 1$ the coupling is exponentially weak, because of the fact that $\kappa_* \cong 2/\epsilon \gg 1$ in the instability window. The boundary wave on one wall produces only an exponentially small disturbance on the other wall. Thus, for the SG equations, the boundary wave on the wall at $y_* = -\frac{1}{2}$ has approximate structure $\hat{p}_*(y) \propto \exp\{-\kappa_*[y_* + \frac{1}{2}]\}$ and, from (2.7) and (2.8), approximate frequency

$$\omega_* = -\frac{k_*}{2} + \frac{k_*}{\epsilon\kappa_*}. \tag{4.1}$$

The other boundary wave, at $y_* = \frac{1}{2}$, has approximate structure $\hat{p}_*(y) \propto \exp\{\kappa_*[y_* - \frac{1}{2}]\}$ and frequency

$$\omega_* = \frac{k_*}{2} - \frac{k_*}{\epsilon\kappa_*}. \tag{4.2}$$

The two frequencies match when $\kappa_* = 2/\epsilon$, consistent with the location of the instability window. Since the boundary waves always propagate with the wall on their right (section 3), this explains why instability can occur only for an *anticyclonic* shear flow. For $|k_*/m_*| \ll 1$ (that is, $|k/m| \ll f/N$), the resulting instability is the coupled Kelvin-wave instability. For $|k_*/m_*| \to \infty$, the resulting instability, in the SG case, is the ''mirage-wave instability.''

In terms of the wave-activity conservation relations used in Kushner and Shepherd (1995a,b), it may be shown that all the SG instability modes have zero pseudomomentum and zero pseudoenergy, essentially because the two boundary waves have opposite signed pseudomomenta. These, of course, are only necessary (Arnol'd-type) and not sufficient conditions for instability.

*Acknowledgments.* This work arose in connection with PJK's Ph.D. thesis at the University of Toronto. PJK is supported by a Natural Sciences and Engineering Research Council of Canada (NSERC) Postdoctoral Fellowship and by NOAA Grant NA67RJ0120. TGS is supported by grants from NSERC and the Atmospheric Environment Service of Canada. MEM's work was supported by a UK SERC/Engineering and Physical Sciences Research Council Senior Research Fellowship. The views expressed herein do not necessarily represent those held by NOAA or any of its subagencies.

## APPENDIX

## Dynamical Equations

### *a. Equations for stability analysis*

For the basic flow described in section 2, the linearized hydrostatic Boussinesq equations under the geo-

strophic momentum approximation (Hoskins 1975)—also known as the semigeostrophic equations—are

$$\tilde{D}u_g' - (f - \tilde{u}_y)v' = -\frac{1}{\rho_0}\frac{\partial p'}{\partial x}, \quad (A.1)$$

$$\tilde{D}v_g' + fu' = -\frac{1}{\rho_0}\frac{\partial p'}{\partial y}, \quad (A.2)$$

$$\frac{\partial p'}{\partial z} = -\rho_0 g\rho', \quad (A.3)$$

$$\frac{\partial u'}{\partial x} + \frac{\partial v'}{\partial y} + \frac{\partial w'}{\partial z} = 0, \quad (A.4)$$

$$\tilde{D}\rho' - \frac{N^2}{g}w' = 0. \quad (A.5)$$

Primes indicate disturbance quantities, $z$ is the geometric height, $\mathbf{u}' = (u', v', w')$ is the disturbance velocity, $p'$ is the disturbance pressure, the density

$$\rho = \rho_0 + \rho_1(z) + \rho_0\rho'(x, y, z, t), \quad (A.6)$$

where $\rho_0$ is a constant, $(u_g', v_g') = (\rho_0 f)^{-1}(-p'_y, p'_x)$ is the disturbance geostrophic velocity, the static stability

$$N^2 = -\frac{g}{\rho_0}\frac{\partial \rho_1}{\partial z}, \quad (A.7)$$

here taken to be constant, and

$$\tilde{D} = \frac{\partial}{\partial t} + \tilde{u}\frac{\partial}{\partial x}. \quad (A.8)$$

The linearized Boussinesq Euler equations are

$$\tilde{D}u' - (f - \tilde{u}_y)v' = -\frac{1}{\rho_0}\frac{\partial p'}{\partial x}, \quad (A.9)$$

$$\tilde{D}v' + fu' = -\frac{1}{\rho_0}\frac{\partial p'}{\partial y}, \quad (A.10)$$

$$\tilde{D}w' = -\frac{1}{\rho_0}\frac{\partial p'}{\partial z} - g\rho', \quad (A.11)$$

and (A.4)–(A.8). Equation (2.10) is derived by taking the horizontal curl of (A.9)–(A.10), the three-dimensional divergence of (A.9)–(A.11), $\partial_x$(A.9)–$\partial_y$(A.10), and $\partial_x$(A.10)+$\partial_y$(A.9), and then cross-substituting the resulting expressions.

### *b. Equations for neutral-wave analysis*

The coordinate rotation for the geometry described in section 3 is

$$\begin{pmatrix} x_1 \\ x_2 \\ x_3 \end{pmatrix} = \begin{pmatrix} \cos\phi & \sin\phi\cos\alpha & \sin\phi\sin\alpha \\ -\sin\phi & \cos\phi\cos\alpha & \cos\phi\sin\alpha \\ 0 & -\sin\alpha & \cos\alpha \end{pmatrix}\begin{pmatrix} x \\ y \\ z \end{pmatrix}. \quad (A.12)$$

The linearized Euler equations for the resting basic state are

$$\partial_t\mathbf{u}' + f\hat{\mathbf{z}}\times\mathbf{u}' = -\frac{1}{\rho_0}\nabla p' - g\rho'\hat{\mathbf{z}}, \quad (A.13)$$

$$\nabla\cdot\mathbf{u}' = 0, \quad (A.14)$$

$$\partial_t\rho' - \frac{N^2}{g}\mathbf{u}'\cdot\hat{\mathbf{z}} = 0, \quad (A.15)$$

where $\nabla = (\partial_{x_1}, \partial_{x_2}, \partial_{x_3})$ and $\mathbf{u}' = (u_1, u_2, u_3)$. In the hydrostatic approximation, the momentum equation (A.13) is replaced by

$$\partial_t(\mathbf{u}' - \mathbf{u}'\cdot\hat{\mathbf{z}}\hat{\mathbf{z}}) + f\hat{\mathbf{z}}\times\mathbf{u}' = -\frac{1}{\rho_0}\nabla p' - g\rho'\hat{\mathbf{z}}, \quad (A.16)$$

and (A.14)–(A.15) remain unchanged. In the semigeostrophic approximation, (A.13) is replaced by

$$\hat{\mathbf{z}}\times\left(\frac{\partial}{\partial t}\frac{\nabla p'}{\rho_0 f} + f\mathbf{u}'\right) = -\frac{1}{\rho_0}\nabla p' - g\rho'\hat{\mathbf{z}}, \quad (A.17)$$

and (A.14)–(A.15) remain unchanged.

For solutions of the form (3.1), the boundary condition that $u'_3$, the component of velocity normal to the wall, must vanish at the wall implies that $u'_3$ must vanish in the interior as well. Since $\partial_{x_1} = 0$ for these solutions, (A.14) with $u'_3 = 0$ implies that $\partial_{x_2}u'_2 = 0$. We here examine solutions for which $u'_2 = 0$. [See Rhines (1970) for comments on solutions with $\partial_{x_2}u'_2 = 0$ and $u'_2 \neq 0$.]

## REFERENCES


Allen, J. S., J. A. Barth, and P. A. Newberger, 1990: On intermediate models for barotropic continental shelf and slope flow fields. Part I: Formulation and comparison of exact solutions. *J. Phys. Oceanogr.,* **20,** 1017–1042.

Cairns, R. A., 1979: The role of negative energy waves in some instabilities. *J. Fluid Mech.,* **92,** 1–14.

Eady, E. T., 1949: Long waves and cyclone waves. *Tellus,* **1,** 33–52.

Hoskins, B. J., 1975: The geostrophic momentum approximation and the semi-geostrophic equations. *J. Atmos. Sci.,* **32,** 233–242.

——, and F. P. Bretherton, 1972: Atmospheric frontogenesis models: Mathematical formulation and solution. *J. Atmos. Sci.,* **29,** 11–37.

——, M. E. McIntyre, and A. W. Robertson, 1985: On the use and significance of isentropic potential-vorticity maps. *Quart. J. Roy. Meteor. Soc.,* **111,** 877–946; Corrigendum, **113,** 402–404.

Kushner, P. J., 1995: A generalized Charney–Stern theorem for semi-geostrophic dynamics. *Tellus,* **47A,** 541–547.

——, and T. G. Shepherd, 1995a: Wave-activity conservation laws and stability theorems for semi-geostrophic dynamics. Part 1. Pseudo-momentum-based theory. *J. Fluid Mech.,* **290,** 67–104.

——, and ——, 1995b: Wave-activity conservation laws and stability theorems for semi-geostrophic dynamics. Part 2. Pseudoenergy-based theory. *J. Fluid Mech.,* **290,** 105–129.

Lighthill, M. J., 1963: Boundary layer theory. *Laminar Boundary Layers,* L. Rosenhead, Ed., Oxford University Press, 46–113.

Press, W. H., S. A. Teukolsky, W. T. Vetterling, and B. P. Flannery, 1994: *Numerical Recipes in FORTRAN.* Cambridge University Press, 963 pp.

Rhines, P., 1970: Edge-, bottom-, and Rossby waves in a rotating stratified fluid. *Geophys. Fluid Dyn.,* **1,** 273–302.

Sakai, S., 1989: Rossby–Kelvin instability: A new type of ageostrophic instability caused by a resonance between Rossby waves and gravity waves. *J. Fluid Mech.,* **202,** 149–176.